Numerical Investigation on Frequency Dependence of Hysteresis Characteristics of Conducting Ferromagnetic Materials

Zhang Yubo[1], Liu Tianyi[2], Liao Zhenyu[3], Li Dong[1], and Chen Dezhi[1(✉)]

[1] State Key Laboratory of Advanced Electromagnetic Engineering and Technology, Huazhong University of Science and Technology, Wuhan 430074, China
dzhchen@hust.edu.cn

[2] State Grid Jiangsu Electric Power Company Suzhou Power Supply Bureau, Suzhou 215004, China

[3] State Grid Hunan Electric Power Company Electric Power Research Institute, Changsha 410007, China

Abstract. The hysteresis characteristics of ferromagnetic materials have significant effects on the performance and loss of electrical devices and components. Studies have shown that the hysteresis loop changes significantly with the increase of frequency, which becomes an important factor in electrical designing and operating. In order to provide a reasonable explanation and analysis method for the variation of dynamic hysteresis loops in the wide frequency range, experimental measurements and theoretical simulations are carried out. In this paper, the change of the hysteresis loop shape caused by the increase of frequency is attributed to eddy currents in the sample, so only the static hysteresis loop is the real reflection of the material characteristics, at which frequency the eddy current effect can be ignored. In order to verify this conjecture, the static hysteresis loops and the dynamic hysteresis loops in the range of 20 Hz ~ 1000 Hz were measured for the annular sample made of 20# steel and B35A300 non-oriented silicon steel sheet. Then, based on the static hysteresis loops of their own, the finite-difference time-domain method was used to solve Maxwell equations at different frequencies to obtain the magnetic field distribution in the sample. The average magnetic induction intensity was used to get the hysteresis loops. The calculated curves are found in good agreement with the measured ones, which indicates that the loop swelling-up is due to the inaccuracy of the measurement principle, and frequency has no effect on the hysteresis characteristics of 20# steel and B35A300 non-oriented silicon steel sheet at least in the frequency range below 1 kHz.

Keywords: Magnetic hysteresis loop · Frequency characteristic · Maxwell equations · Numerical simulation

1 Introduction

The electrical system contains a large number of magnetic devices and components made of ferromagnetic material, which plays an important part in the transformation process

C. Ma et al. (Eds.): ICWPT 2022, LNEE 1018, pp. 1057–1068, 2023.
https://doi.org/10.1007/978-981-99-0631-4_106

of electric energy [1–4]. But the nonlinearity and loss of ferromagnetic materials also directly affect the quality of electric energy and the stability of electrical system [5]. Previous studies have shown that the hysteresis loops of ferromagnetic materials exhibit different shapes under different operating frequencies and waveforms [5–8]. So the prediction of dynamic hysteresis loop of ferromagnetic materials is of great importance to the optimal design and stable operation of magnetic devices and components [6, 9–11].

Most of the existing methods for predicting dynamic hysteresis loops are based on dynamic hysteresis models, such as the dynamic Preisach hysteresis model [12–15], the dynamic Jiles-Atherton (J-A) hysteresis model [8, 16, 17] and the dynamic Energetic hysteresis model [18–21], which are evolved from their static hysteresis models respectively.

The above dynamic hysteresis models all need to measure the data in similar working conditions in advance, and then to identify the undetermined parameters of the model. Therefore, the model is in essence a fitting method, which cannot predict the dynamic hysteresis loop physically.

Based on the analysis of experimental data, we speculate that the change of the measured dynamic hysteresis loops with increase of frequency is essentially caused by the imperfection of the measurement principle, which does not take into account the eddy current effect in the test sample under dynamic conditions. In order to verify the above speculation, we select 20# steel and B35A300 non-oriented silicon steel, which are commonly used in electric motors, and measure their static hysteresis loops and dynamic hysteresis loops in the range of 20 Hz ~ 1000 Hz. Then we calculate the dynamic hysteresis loops by solving Maxwell equations using finite-difference time-domain (FDTD) method based on the static hysteresis loops, and compare them with the measurements. The result shows that the change of measured dynamic hysteresis loops with frequency can be explained by the inhomogeneity of magnetic field caused by eddy currents, without introducing other assumptions, which indicates that the essential hysteresis characteristics of ferromagnetic materials do not change with frequency at least in the frequency range below 1 kHz.

2 Measurement Devices and Measurement Results

2.1 Measurement Devices and Measurement Principle

The experimental materials we choose are 20# steel ring and B35A300 non-oriented silicon steel sheet, whose main parameters are shown in Tables 1 and 2. 20# steel ring is wrapped by coil (see Fig. 1), and then measured by the ring sample measurement method. B35A300 non-oriented silicon steel sheets are placed into Epstein frame (see Fig. 2), and then measured by Epstein frame measurement method. We choose MATS-2010SD and MATS-3000M as our measurement devices, whose principles are shown in Fig. 3.

The magnetic field strength we measure is defined as follows:

$$H = \frac{N_1 i_1}{l_m} \tag{1}$$

Table 1. The main parameters of 20# steel ring.

Parameter	Describe	Value
d	Inside diameter	68.0 mm
D	Outside diameter	76.4 mm
h	Thickness	4.0 mm
γ	Conductivity	4.6×10^6 S/m
N_1	Number of turns of primary coil	200
N_2	Number of turns of secondary coil	50

Table 2. The main parameters of B35A300 non-oriented silicon steel sheet.

Parameter	Describe	Value
a	Length	300.0 mm
b	Width	30.0 mm
c	Thickness	0.350 mm
n	Number of sheets	24
γ	Conductivity	3.18×10^6 S/m
N_1	Number of turns of primary coil	700
N_2	Number of turns of secondary coil	700

Fig. 1. 20# steel ring and the coils.

where N_1 is the number of turns of primary coil, i_1 is the current of primary coil, and l_m is the length of magnetic path.

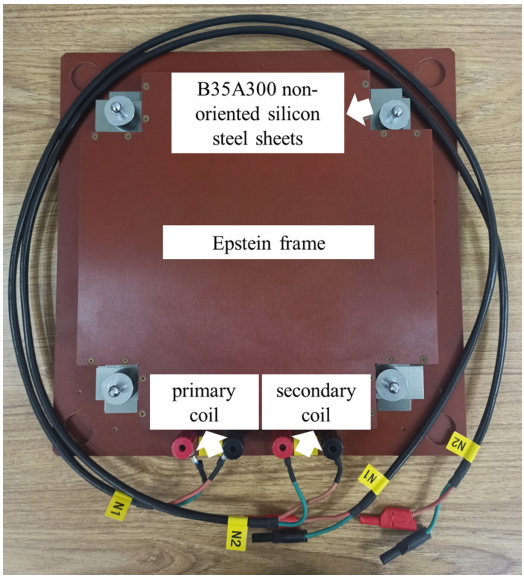

Fig. 2. B35A300 non-oriented silicon steel sheets and Epstein frame.

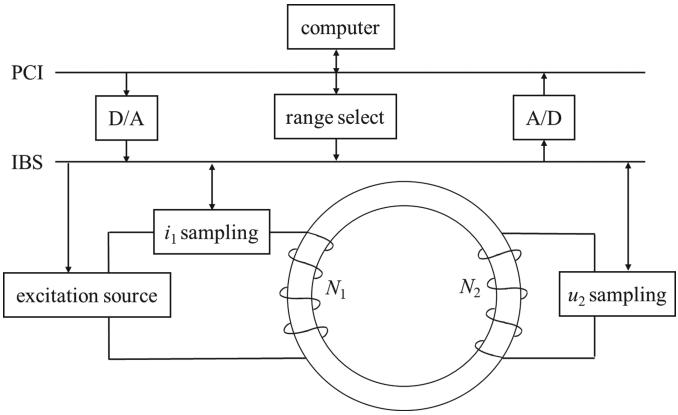

Fig. 3. The measuring principles of the measuring devices.

The magnetic flux density is defined as follows:

$$B = \frac{1}{N_2 S_m} \int u_2 \mathrm{d}t \tag{2}$$

where N_2 is the number of turns of secondary coil, S_m is the cross section area of magnetic path, u_2 is the voltage of secondary coil, and t is the time.

The magnetic field strength and the magnetic flux density are obtained by Eq. (1) and (2), and then we can draw the hysteresis loop.

2.2 Measurement Results

By changing the current of primary coil, we can obtain the hysteresis loops at different conditions. The measured static hysteresis loops of 20# steel ring and B35A300 non-oriented silicon steel sheet are shown in Figs. 4 and 5, respectively. These curves will be used to predict the dynamic hysteresis loops at different frequencies in the next section. The measured dynamic hysteresis loops will be compared with the predicted ones in Sect. 5 (see Figs. 8 and 9).

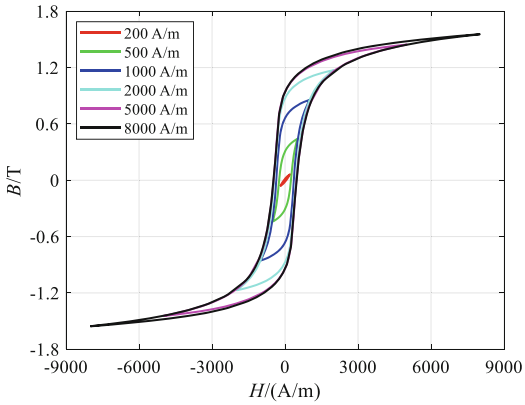

Fig. 4. A series of static hysteresis loops measured at different maximum magnetic field strength of 20# steel ring with a very low frequency (<0.1 Hz).

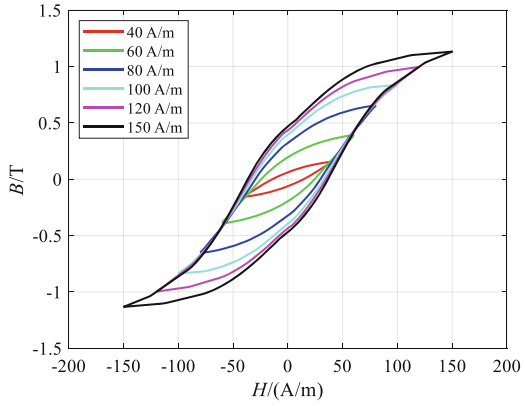

Fig. 5. A series of static hysteresis loops measured at different maximum magnetic field strength of B35A300 non-oriented silicon steel sheet with a very low frequency (<0.1 Hz).

3 Theory Analysis

Now let's take a closer look at Eqs. (1) and (2) used to calculate the magnetic field strength H and magnetic flux density B in measurements.

Equation (1) is derived from Ampere's circuital law, and Eq. (2) is derived from Faraday's law of electromagnetic induction. Both formulas imply that the magnetic field in the sample is uniformly distributed, which is true at DC or very low frequencies. However, under dynamic conditions, eddy currents in the sample cause this assumption to fail.

In this case, H in Eq. (1) is just H on the sample surface, while B in Eq. (2) is the average value of B on the sample section. Considering the effect of the eddy current, the B amplitude inside the conductor is smaller than the B of the surface, and the phase also lags behind the B of the surface. The same is true for the mean of B across the cross section, and the higher the frequency, the more significant this feature becomes.

If we observe the measured dynamic hysteresis loops, we will find the same rule: as the frequency increases, the peak of B decreases, and the position of the B peak occurrence lags behind that of the H peak. The higher the frequency, the more pronounced the phenomenon is.

Therefore, it is reasonable to speculate that the shape change of the measured hysteresis loop with frequency is due to eddy currents not considered in the measurement. The true hysteresis characteristics of the material will most likely not vary with the frequency. In other words, only the static hysteresis loop measured at DC or very low frequency is the true description of the physical characteristics of the material, and the dynamic hysteresis loop measured at high frequency is contaminated by the vortex effect.

To verify this, in the next section, we will use the FDTD method to solve Maxwell equations based on the static hysteresis loops, to obtain the actual magnetic field distribution on the cross section and to get the average B to draw the B-H curves, and compare them with the measured ones.

4 Calculation Model

20# steel ring and the coils are roughly a symmetric model. Since the size of the section is much smaller than the radius of the ring, to simplify the calculation, the section of the ring can be approximated as the rectangular region in Cartesian coordinate system as the solution region (see Fig. 6).

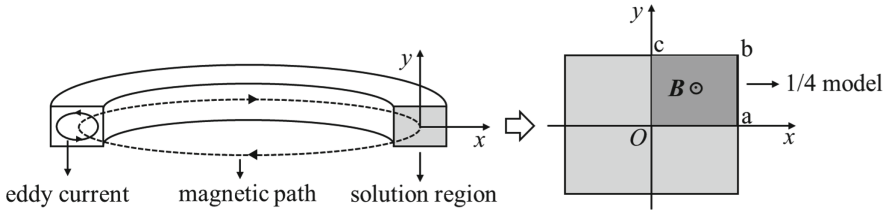

Fig. 6. Simplification of the computational model of 20# steel ring.

Ignoring the displacement current, Maxwell equations are simplified as:

$$\begin{cases} \nabla \times E = -\frac{\partial B}{\partial t} \\ \nabla \times H = \gamma E \end{cases} \tag{3}$$

where $\boldsymbol{E}$ is the electric field strength vector, $\boldsymbol{B}$ is the magnetic flux density vector, t is the time, $\boldsymbol{H}$ is the magnetic field strength vector, and γ is the conductivity of the sample. $\boldsymbol{B} = \boldsymbol{B}(\boldsymbol{H})$ is determined by the static hysteresis loops shown in Fig. 4. $\boldsymbol{H}$ only has a z component ($\boldsymbol{H} = H\boldsymbol{e}_z$), so we can get rid of $\boldsymbol{E}$:

$$\frac{\partial^2 H}{\partial x^2} + \frac{\partial^2 H}{\partial y^2} = \gamma \frac{\partial B}{\partial H} \frac{\partial H}{\partial t} \tag{4}$$

Because of the symmetry, we choose the 1/4 model for calculation, which means that the Oabc region in Fig. 6 is used as the final solution region.

On ab and bc, the boundary conditions are imposed as follows:

$$H|_{\mathrm{ab}} = H|_{\mathrm{bc}} = H_{\mathrm{s}}(t) \tag{5}$$

where $H_{\mathrm{s}}(t)$ is the magnetic field strength waveform corresponding to each dynamic hysteresis loop and is obtained by recording the current of primary coil.

On Oa and Oc, due to the symmetry, the boundary conditions are imposed as follows:

$$\left.\frac{\partial H}{\partial y}\right|_{O\mathrm{a}} = \left.\frac{\partial H}{\partial x}\right|_{O\mathrm{c}} = 0 \tag{6}$$

At the initial time, the sample is in a completely demagnetized state:

$$H(x, y, t)|_{t=0} = 0 \tag{7}$$

In the calculation, the value of $B = B(H)$ needs to be obtained by interpolation from the static hysteresis loops shown in Fig. 4. In an excitation cycle, $H_{\max}$ of each point in the solution region is different, so the static hysteresis loop of each point is also different. $H_{\max}$ of each point is determined by iterating, which determines its static hysteresis loop. The data required for the calculation usually doesn't come from the known static hysteresis loops. However, the change of the static hysteresis loop changes with $H_{\max}$ continuously, so we can get the desired static hysteresis loop from the known static hysteresis loops. The interpolation method of the static hysteresis loop is shown in Fig. 7: firstly, according to the value of $H_{\max}$, find the known B_1-H_1 curve and B_3-H_3 curve which adjacent to the desired B_2-H_2 curve; secondly, according to a same waveform style (such as cosine) and the value of $H_{\max 1}$, $H_{\max 2}$ and $H_{\max 3}$, spread H_1, H_2 and H_3 into a same time cycle, respectively; thirdly, map H1 to B1 from B_1-H_1 curve, and map H3 to B3 from B_3-H_3 curve; then, according to the value of $B_{\max 1}$, $B_{\max 2}$ and $B_{\max 3}$, determine the linear interpolation ratio, and use B_1 and B_3 to get B_2; finally, according to H_2 and B_2, get the desired B_2-H_2 curve.

The FDTD method is used to solve the problem of initial conditions and the boundary conditions that composed of Eq. (4) to Eq. (7), so we can get the magnetic field strength and the magnetic flux density at any point and at any time in the sample. For B35A300 non-oriented silicon steel sheet, we only need to select the cross section of one piece for calculation in a similar way (because of its large ratio of width to thickness, the dimension of calculation can even be reduced).

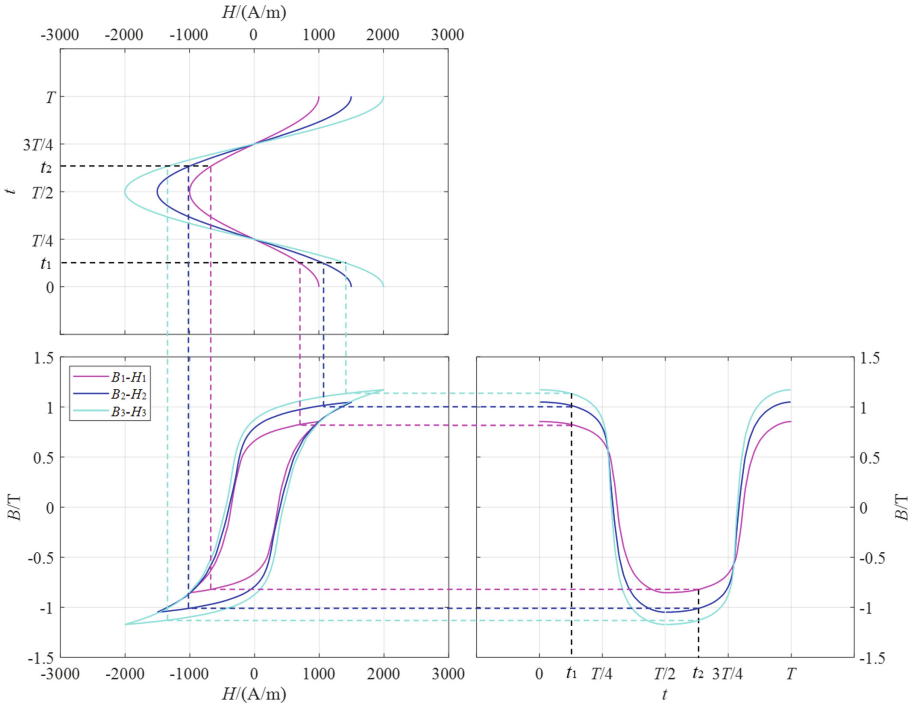

Fig. 7. The interpolation method of the static hysteresis loop.

5 Comparison of Calculation Results and Measurement Results

According to the calculation results, draw the $\overline{B}$-H_s curves, and compare it with the measurement results. In the calculation curve, H_s is the magnetic field strength on the surface of sample, and $\overline{B}$ is the magnetic flux density on the cross section of magnetic path, which can be calculated as follows:

$$\overline{B}(t) = \frac{1}{S_m} \iint_S B(x, y, t) \mathrm{d}x\mathrm{d}y \tag{8}$$

where S is the cross section region of magnetic path.

We calculate the dynamic hysteresis loops of 20# steel ring and B35A300 non-oriented silicon steel sheet at different frequencies. The comparison of the calculated hysteresis loops and the measured hysteresis loops of the two samples at different frequencies is shown in Figs. 8 and 9 respectively.

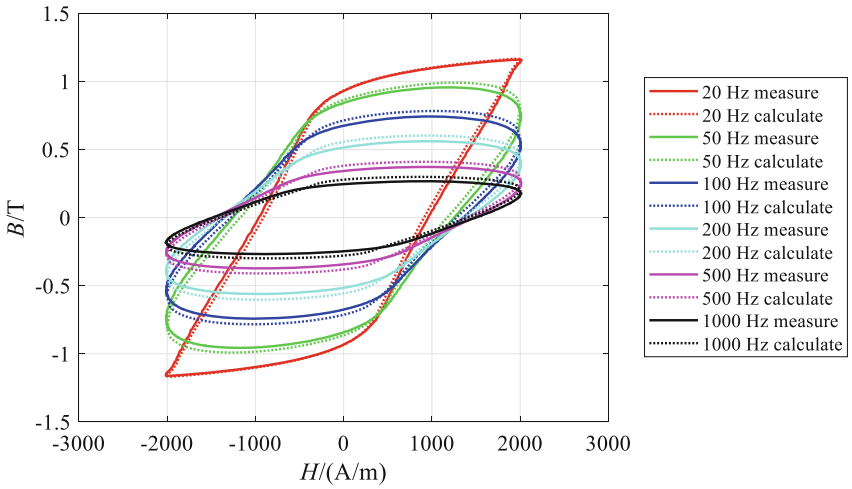

(a) H_{max}=2000 A/m.

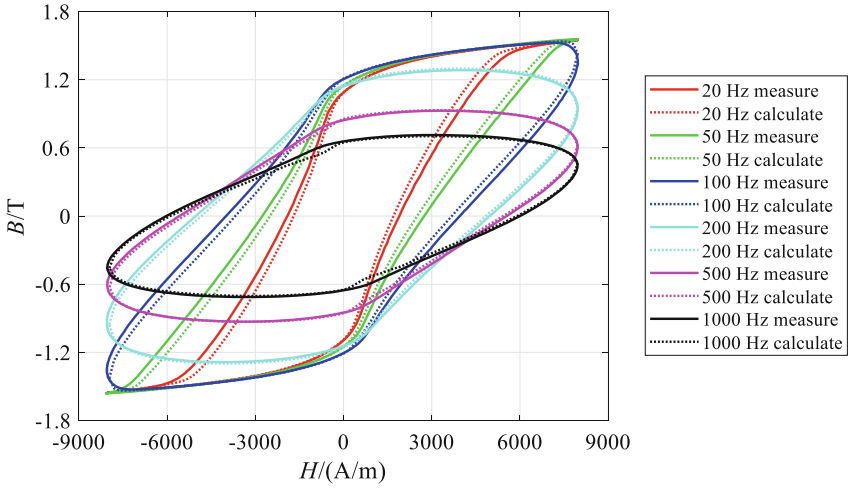

(b) H_{max}=8000 A/m.

Fig. 8. Comparison of dynamic hysteresis loops between the calculated one and the measured one of 20# steel ring at different frequencies.

The result shows that in the frequency range calculated in this paper, the calculated hysteresis loops of 20# steel ring and B35A300 non-oriented silicon steel sheet are in good agreement with the measured hysteresis loops, and the trend of *B-H* curve which changes with frequency is almost the same. This has verified the speculation about the hysteresis characteristics in this paper: at least in the frequency range below 1 kHz, the frequency has no effect on the hysteresis characteristics of 20# steel ring and B35A300 non-oriented silicon steel sheet, and the effect of frequency on the hysteresis loop is caused by the imperfect measurement principle.

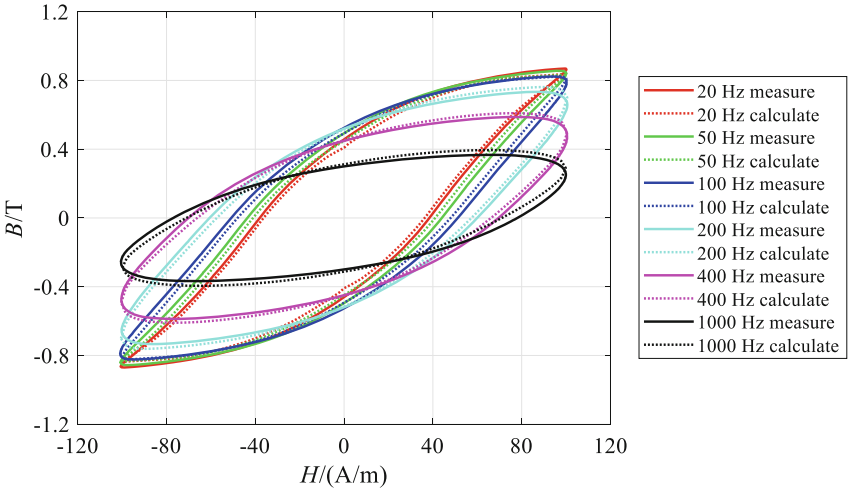

(a) H_{max}=100 A/m.

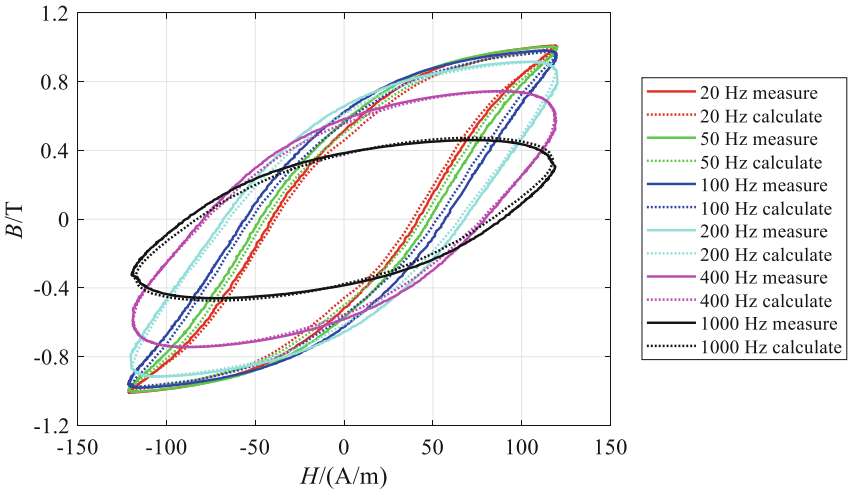

(b) H_{max}=120 A/m.

Fig. 9. Comparison of dynamic hysteresis loops between the calculated one and the measured one of B35A300 non-oriented silicon steel sheet at different frequencies.

6 Conclusions

In this paper, we select the annular sample made of 20# steel which is commonly used in motors and B35A300 non-oriented silicon steel commonly which is commonly used in electric vehicles as 2 examples. According to their static hysteresis loops measured at a very low frequency (<0.1 Hz) where the eddy current effect can be ignored, we use numerical method to solve Maxwell equations without introducing other assumptions, and then we get the way that the magnetic field in the sample changes with the excitation.

Then, we use H_s which is the magnetic field strength on the surface of sample and $\overline{B}$ which is the magnetic flux density on the cross section of magnetic path to draw the $\overline{B}$-H_s curves. The result shows that at least in the frequency range below 1 kHz, the calculated hysteresis loops are in good agreement with the measured hysteresis loops.

At least in the frequency range below 1 kHz, the frequency has no effect on the hysteresis characteristics of 20# steel and B35A300 non-oriented silicon steel sheet, or we can say that the change of the magnetic domain's orientation completely keeps up with the change of the magnetic field caused by the external excitation. And the change of the dynamic hysteresis loops is caused by the imperfect measurement principle, rather than the electromagnetic characteristics of the material itself.

The method in this paper solves Maxwell equations directly and doesn't introduce other assumptions, so it can be considered that it gives a physical explanation for that the dynamic hysteresis loops changes with the frequency.

Acknowledgments. This work was funded by the National Natural Science Foundation of China (11775088).

References

1. Zhi, Z.G., Bi, Z.L.: Improvement and verification of ferromagnetic material loss model under sinusoidal and harmonic excitation. Proc. CSEE **42**(09), 2452–3460 (2022). (in Chinese)
2. Sun, H., Li, Y.J., Liu, H., Wan, Z.Y.: The calculation method of nanocrystalline core loss under non-sinusoidal excitation and experimental verification. Trans. China Electrotechnical Soc. **37**(04), 827–836 (2022). (in Chinese)
3. Zhao, B., Song, Q., Liu, W.H., et al.: Overview of dual-active-bridge isolated bidirectional DC-DC converter for high-frequency-link power-conversion system. IEEE Trans. Power Electron. **29**(8), 4091–4106 (2014)
4. Liu, R., Li, L., Qiao, G.Y., Jin, Y.J., Li, Y.L.: Calculation method of magnetic material losses under non-sinusoidal excitation considering the biased minor loops. Proc. CSEE **40**(19), 6013–6093 (2022). (in Chinese)
5. Zhi, Z.G., Lin, Q.M., Ji, J.A., Ma, X.W.: Wideband loss separation models of ferromagnetic materials considering skin effect. Proc. CSEE **42**(14), 5374–5383 (2022). (in Chinese)
6. De, B.O., Ragusa, C., Appino, C., et al.: Prediction of energy losses in soft magnetic materials under arbitrary induction waveforms and DC bias. IEEE Trans. Ind. Electron. **64**(3), 2522–2529 (2017)
7. Li, Y.J., Li, Y.T., Lin, Z.W., Cheng, Z.G., Tian, Y.K., Chen, R.Y.: An improved bouc-wen based hysteresis model under harmonic magnetization. Trans. China Electrotechnical Soc. **37**(17), 4259–4268 (2022). (in Chinese)
8. Zhi, Z.G., Ma, X.W., Ji, J.A.: Simulation and verification on hysteresis characteristics of electrical steel under sinusoidal and DC bias conditions considering frequency effects. Proc. CSEE **41**(23), 8178–8187 (2021). (in Chinese)
9. Raulet, M.A., Ducharne, B., Masson, J.P., et al.: The magnetic field diffusion equation including dynamic hysteresis: a linear formulation of the problem. IEEE Trans. Magn. **40**(2), 872–875 (2004)
10. De, B.O., Ragusa, C., Appino, C., et al.: A computationally effective dynamic hysteresis model taking into account skin effect in magnetic laminations. Physica B **435**(1), 80–83 (2014)

11. Beatrice, C., Appino, C., De, B.O., et al.: Broadband magnetic losses in Fe-Si and Fe-Co laminations. IEEE Trans. Magn. **50**(4), 1–4 (2014)
12. Mayergoyz, I.D.: Mathematical models of hysteresis. IEEE Trans. Magn. **22**(5), 603–608 (1986)
13. Bertotti, G.: Dynamic generalization of the scalar preisach model of hysteresis. IEEE Trans. Magn. **28**(5), 2599–2601 (1992)
14. Zhao, Z.G., Li, X.X., Ji, J.A., Wei, L., Wen, T.: Simulation of magnetic properties of electrical steel sheets based on preisach model. High Vol. Eng. **45**(12), 4038–4046 (2019). (in Chinese)
15. Zhao, Z.G., Zhang, P., Ma, X.W., Hu, X.J., Xu, M.: Simulation of magnetic properties of electrical steel sheets based on improved preisach model. High Volt. Eng. **47**(06), 2149–2157 (2021). (in Chinese)
16. Jiles, D., Atherton, D.: Ferromagnetic Hysteresis. IEEE Trans. Magnetics **19**(5), 2183–2185 (1983)
17. Zhi, Z.G., Ma, X.W., Ji, J.A.: Parameter identification and verification of J-A dynamic hysteresis model based on hybrid algorithms of AFSA and PSO. Chin. J. Sci. Instrum. **41**(01), 26–34 (2020). (in Chinese)
18. Hauser, H.: Energetic model of ferromagnetic hysteresis. J. Appl. Phys. **75**(5), 2584–2597 (1994)
19. Hauser, H.: Energetic model of ferromagnetic hysteresis 2: magnetization calculations of (110) [001] fesi sheets by statistic domain behavior. J. Appl. Phys. **77**(6), 2625–2633 (1995)
20. Hauser, H.: Energetic model of ferromagnetic hysteresis: isotropic magnetization. J. Appl. Phys. **96**(5), 2753–2767 (2004)
21. Liu, R., Li, L.: A dynamic energetic hysteresis model based on the field separation approach and statistical theory of losses. Proc. CSEE **39**(21), 6412–6419 (2019). (in Chinese)